

Bifurcations Induced by Periodic Forcing and Taming Chaos in Dripping Faucets

Ken KIYONO* and Nobuko FUCHIKAMI

Department of Physics, Tokyo Metropolitan University, Tokyo 192-0397

(Received June 26, 2001)

Using a mass-spring model, we study a periodically forced dripping faucet as an example of nonfeedback control systems. The model is confirmed to exhibit entrainment from chaotic to periodic motion by adding an external force, which has been observed experimentally. It is found from an analysis of a two-dimensional Poincaré map that a discontinuous change between chaotic and periodic motion occurs via global bifurcations including a homoclinic bifurcation and a homoclinic tangency crisis. A hysteresis of the transition point is also explained. A possible way of suppressing chaos in the dripping faucet system by periodic forcing is suggested from the mass-spring model, which is also supported by a corresponding fluid dynamical simulation.

KEYWORDS: leaky faucet dynamics, controlling chaos, homoclinic bifurcation, homoclinic tangency crisis, entrainment

DOI: 10.1143/JPSJ.71.49

1. Introduction

Chaos occurs widely in engineering and natural systems. In the past few years practical implementations of controlling chaos have been studied with great interest.^{1–6)} Such control schemes can be divided broadly into two categories, *feedback* control and *nonfeedback* control. The pioneering work on controlling chaos by Ott, Grebogi, and Yorke (OGY method)²⁾ is a representative example of feedback control systems. The OGY method aims to stabilize one of many unstable periodic orbits embedded in the chaotic attractor through small time-dependent perturbations in an accessible system parameter. Although the OGY method is very general, it is difficult for some high-speed systems to implement the control procedure. In the nonfeedback control systems, on the other hand, the applied perturbation is independent of the state of the system. So far, controlling chaos by applying a suitable weak periodic perturbation, which is sometimes called *taming chaos*,³⁾ has been studied in a variety of chaotic dynamical systems both theoretically^{4–7)} and experimentally.⁸⁾ Recently, analyzing a constrained system in which a one-dimensional Poincaré map is derived, Tamura *et al.*⁴⁾ showed that taming chaos occurs by a saddle node bifurcation. However, many issues in the nonfeedback control scheme are still not well understood, for example, phase effect,⁶⁾ phase diagram structures,⁵⁾ bifurcation structures for higher-dimensional dynamical systems,⁵⁾ etc.

Recently, Ilaraza–Lomel *et al.* applied the OGY method to a dripping faucet system. They suggested a possible way of controlling chaos using a magnetorheological fluid in place of the customary water. On the other hand, an influence of periodic forcing on a dripping (water) faucet has been investigated experimentally by Shoji.²⁷⁾ He found that a periodic external force can induce a transition from periodic to chaotic (instead of chaotic to periodic) motion. Motivated by these studies, we investigate in this paper a dripping faucet system under the influence of periodic forcing.

A dripping faucet system without any perturbation has been studied intensively^{9–24,27)} since Shaw¹⁰⁾ found the first experimental evidence of chaotic behavior, and proposed a mass-spring model for this system. Shaw's model exhibits periodic and chaotic oscillations which look somewhat similar to experimental observations. However, any direct link between such a simple model and the complex mechanisms of drop formation had not been clarified until recently.

In our previous work,^{9,22)} we performed a fluid dynamical simulation based on a new algorithm in order to know how any simple model can mimic the real dripping faucet systems. The results of the simulation successfully reproduced not only deformation of the liquid but also various dynamical behavior observed experimentally. A detailed analysis of the simulation results made it possible to reconstruct a more realistic mass-spring model. The improved mass-spring model thus obtained reproduced experimental results in good qualitative agreement in a wide range of the flow rates; and a variety of complex dynamical behavior can be systematically explained in terms of a low-dimensional dynamical system.

We apply the improved mass-spring model to a dripping faucet system under a periodic force. We first confirm in §2 that the model can well reproduce a bifurcation diagram obtained from the experiment of a periodically forced dripping faucet. We then numerically analyze, in §3, bifurcations induced by periodic forcing. The periodic external force is shown to induce discontinuous changes from chaotic to period-one (P1) motion. A hysteresis of the transition points between chaos and P1 motion is observed depending on whether the forcing amplitude is increased or decreased. Such sudden changes usually do not occur for the same system without periodic forcing. It turns out from an analysis of a Poincaré map that a homoclinic bifurcation and a homoclinic tangency crisis (boundary crisis) are essential to suppress the chaotic motion, which had not been realized so far. In §4, we present a fluid dynamical simulation which shows similar changes from chaotic to P1 behavior as predicted by the mass-spring model.

*E-mail: k.kiyono@phys.metro-u.ac.jp

2. Effects of Periodic Forcing on the Dripping Faucet

First of all, we confirm that our mass-spring model can reproduce the dynamical characteristics of a periodically forced dripping faucet observed experimentally. To our knowledge, any study of periodically forced dripping faucet systems has not been reported, except for Shoji's experiment.²⁷⁾ In his experiment, a periodically oscillating speaker was set on the top of the faucet as shown in Fig. 1, and dripping time intervals $\{T_n\}$ between successive drops were measured. For tiny faucets (diameter ~ 1 mm) and sufficiently slow flow rates Q without any periodic perturbation the time series $\{T_n\}$ are almost equal at each flow rate [Fig. 2 (a)]. In contrast, when the speaker oscillates periodically [Fig. 2(b)], the time series $\{T_n\}$ are distributed over a finite range for various flow rates. In Fig. 2(b) one can see sudden changes from P1 to chaotic motion together with period-doubling bifurcations from P1 to P2. Moreover, frequency entrainments are observed over a certain range of the flow rate: for example, P1 motion with period $T_n = 4\tau$ is indicated in Fig. 2(b), where τ is the forcing period.

Our mass-spring model can reproduce a bifurcation diagram in good qualitative agreement with the experimental observations (Fig. 2), as shown in Fig. 3. The mass-spring model (see ref. 9 for details) with a periodic external force is described by the following equations:

$$\frac{d}{dt} \left(m \frac{dz}{dt} \right) = -kz - \gamma \frac{dz}{dt} + mg + A \sin \left(\frac{2\pi t}{\tau} \right), \quad (2.1)$$

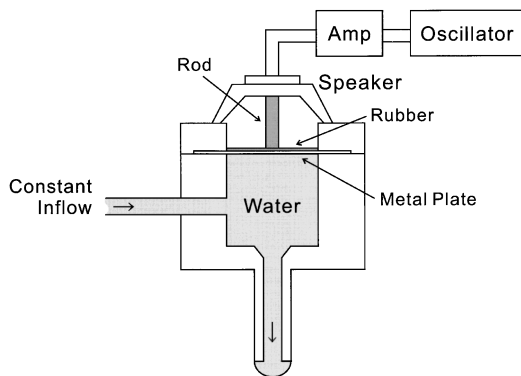


Fig. 1. Schematic setup of a dripping faucet in Shoji's experiment.²⁷⁾

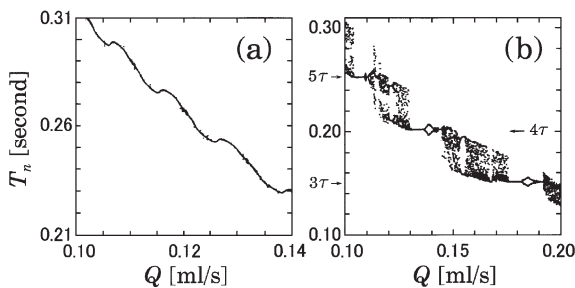


Fig. 2. Bifurcation diagrams in a dripping faucet experiment (a) without and (b) with periodic forcing. The faucet is 1.0 mm in inner diameter, 1.6 mm in outer diameter. In (b) the forcing period $\tau = 0.05$ s. (Reprinted by courtesy of Professor M. Shoji.²⁷⁾)

where z is the center of mass of the forming drop, m is its mass, and g is the gravitational acceleration. Throughout the paper the units of the length, time, and mass are chosen as $l_0 \equiv \sqrt{\Gamma/\rho g}$ ($= 0.27$ cm), $t_0 \equiv (\Gamma/\rho g^3)^{1/4}$ ($= 0.017$ s), and $m_0 \equiv \rho l_0^3$ ($= 0.020$ g), respectively, where Γ is the surface tension, ρ is the density. (The numbers in parenthesis correspond to the water at 20°C). Using these units, one can set $g = 1$ in eq. (2.1). The damping parameter γ was chosen as $\gamma = 0.008$. The drop mass increases linearly with time:

$$\frac{dm}{dt} = \pi a^2 v_0 = \text{const.}, \quad (2.2)$$

where a is the radius of the faucet, and v_0 is the flow velocity. The term $-kz$ represents a surface tension effect of a drop and the spring constant k depends on the mass (i.e., the shape of the drop) as

$$k(m) = \begin{cases} 3.1m^{-0.58} & (m < 0.584) \\ -31m^2 + 32m - 3.88 & (0.584 \leq m < 0.891) \\ 0 & (m \geq 0.891) \end{cases} . \quad (2.3)$$

The above mass dependence of the spring constant k was obtained from the corresponding fluid dynamical simulation⁹⁾ (without periodic forcing) for $a = 0.183$. After k reaches zero ($m \geq 0.891$), the drop undergoes free-fall until the breakup moment, which corresponds to the necking process of the fluid. An important difference of our mass-spring model from others^{10,24-26)} is that the necking process is taken into account explicitly. Breakup of a drop is described in the mass-spring model by assuming that a part of the mass is lost when the position z reaches a critical point z_{crit} . The remnant mass m_r under the faucet is renewed as

$$m_r = Bm + C, \quad \text{when } z = z_{\text{crit}}, \quad (2.4)$$

depending on the total mass m at the breakup moment, where $B = 0.068$ and $C = -0.053$. The position and the velocity just after a breakup moment are renewed as

$$\left. \begin{aligned} z &= z_0 \\ \dot{z} &= v_0 \end{aligned} \right\} \text{ when } z = z_{\text{crit}}. \quad (2.5)$$

The breakup position z_{crit} , the renewed position z_0 and the velocity v_0 were assumed as constant: $z_{\text{crit}} = 4$, $z_0 = 0.15$ and $v_0 = 0$. The relations (2.3), (2.4) and the above

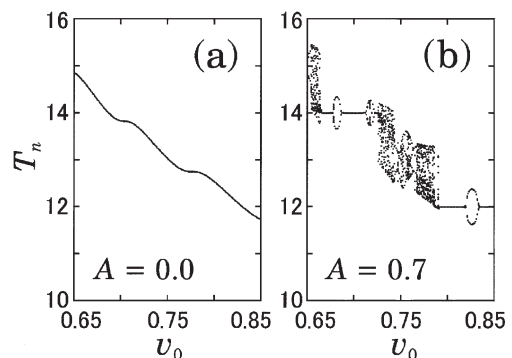


Fig. 3. Bifurcation diagrams obtained from the mass-spring model. (a) the unperturbed system. (b) $A = 0.7$. The faucet radius $a = 0.183$ corresponds to 1.0 mm in diameter. $\tau = 2$ ($= 0.034$ s).

parameter values were obtained by referring to the results of the fluid dynamical simulation.

Comparison between Fig. 2 and Fig. 3 indicates that the present model can well reproduce the qualitative aspects of the experimental results for the dripping faucet under periodic forcing. Moreover, this simple model allows one to analyze the dynamics of the system in terms of a low-dimensional map. When no periodic force is applied ($A = 0$), the remnant mass at the breakup moment, $m_{r,n+1}$, is uniquely determined only by the previous remnant mass $m_{r,n}$ as shown in ref. 9). That is, Poincaré map is defined as a one-dimensional map function $m_{r,n+1} = M(m_{r,n})$, because, just after a breakup moment, the initial conditions of eq. (2.1) are set to be $m_{r,n}$, z_0 and v_0 , where z_0 and v_0 are constants. Accordingly, the dripping time interval T_n is also uniquely determined from $m_{r,n}$: $T_{n+1} = G(m_{r,n})$. Note that the dynamics of $m_{r,n}$ and that of T_n are not topologically conjugated unless the inverse $G^{-1}(T_{n+1})$ exists. In fact, G^{-1} is multivalued, and so is the return map of T_n , namely,

$$\begin{aligned} T_{n+1} &= G(m_{r,n}) \\ &= G(M(m_{r,n-1})) \\ &= G(M(G^{-1}(T_n))) \equiv H(T_n) \end{aligned}$$

is multivalued. To avoid this seeming complexity for the return map of T_n , one may analyze the single valued map function $M(m_{r,n})$.

Figure 4 shows a typical example of the Poincaré map of $m_{r,n}$ obtained numerically from the mass-spring model without periodic forcing ($A = 0$). The map $M_{v_0}(m_{r,n})$ is an oscillating function of $m_{r,n}$, and is shifted to the lower left as the flow velocity v_0 increases. The bifurcation diagram in Fig. 3(a) is understood in terms of this map function: No bifurcation occurs because the stability coefficient $\lambda \equiv M'_{v_0}(m_{r,*})$ at the fixed point $m_{r,*}$ satisfies $|\lambda| < 1$ for v_0 in the range corresponding to Fig. 3(a). In addition, oscillating behavior of $M_{v_0}(m_{r,n})$ is reflected in the oscillation of the T_n vs. v_0 plot.

When a periodic force is applied, the Poincaré map just after the breakup moment is two dimensional because of an additional degree of freedom, the phase of the external force. The map function is then expressed as

$$\begin{pmatrix} m_{r,n+1} \\ \theta_{n+1} \end{pmatrix} = \mathbf{M} \begin{pmatrix} m_{r,n} \\ \theta_n \end{pmatrix}, \quad (2.6)$$

where

$$\theta = \frac{t}{\tau} \text{ modulo } 1.$$

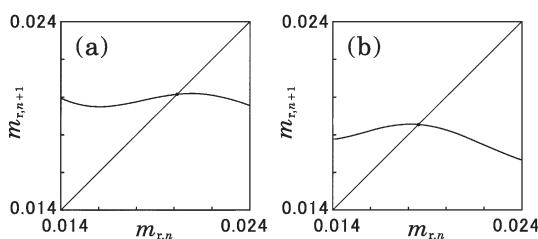


Fig. 4. Map function $m_{r,n+1} = M_{v_0}(m_{r,n})$ obtained from the mass-spring model without periodic forcing ($A = 0$). (a) $v_0 = 0.78$. (b) $v_0 = 0.80$.

Now, the entrainment observed in Fig. 3(b) can be explained as follows. Let $x \equiv (m_r, \theta)$ be a state point on the Poincaré section just after the breakup moment [eq. (2.6)], and let $\bar{x} \equiv (\bar{m}_r, \bar{\theta})$ be a P1 orbit satisfying $\bar{x} = \mathbf{M}(\bar{x})$. Let us note that the period of P1 motion under periodic forcing must be an integer multiple of the forcing period: $T_n = N\tau = \text{const}$. Then the linear relation eq. (2.4) yields an explicit expression for $m_{r,n} = \bar{m}_r$:

$$\bar{m}_r = \frac{BQN\tau + C}{1 - B}, \quad (2.7)$$

where $Q = \pi a^2 v_0$. The fixed point \bar{x} corresponding to P1 motion should satisfy

$$\bar{x} \in I \cap \mathbf{M}(I), \quad (2.8)$$

where $I \equiv \{(m_r, \theta) \mid m_r = \bar{m}_r\}$, and the entire line I is mapped onto a curve $\mathbf{M}(I)$. For a specified value of the integer N , P1 orbits are obtained from eq. (2.7). Figure 5 illustrates how the P1 orbits with $N = 6$ are generated as the flow velocity v_0 is increased from $v_0 = 0.78$ to $v_0 = 0.80$ in Fig. 3(b), where I , and $\mathbf{M}(I)$ are shown by a dashed line, and a solid curve, respectively. As v_0 increases, I is shifted to the right and $\mathbf{M}(I)$ to the left and then they intersect. As will be illustrated in detail in the next section, two P1 orbits corresponding to the intersection points \bar{x}_0 and \bar{x}_1 are generated via a saddle-node bifurcation; \bar{x}_0 is stable and \bar{x}_1 is unstable at $v_0 = 0.78$. In the range of v_0 where $\mathbf{M}(I)$ intersects I , the dripping time intervals $\{T_n\}$ are entrained to an integer multiple of the forcing period τ : $T_n = N\tau$ (P1). [After period doubling, the P2 motion should satisfy $T_n + T_{n+1} = 2N\tau$ (P2).] On the other hand, chaotic motion is realized before the intersection [see Fig. 5(a)].

3. Taming Chaos

As presented in the previous section, the experiment and the model simulation have indicated that the dripping faucet under a periodic force exhibits entrainment, i.e., a sudden change from chaotic to periodic motion as the flow rate Q (or equivalently, the flow velocity v_0) is varied. This easily suggests that chaotic motion for a fixed value of Q might also be entrained to periodic motion if a parameter of the periodic force, say, the amplitude A , is controlled (taming chaos). In this section, we investigate the dynamics of taming chaos in the dripping faucet system using the mass-spring model.

So far, many experimental and theoretical studies have confirmed that dripping faucet systems without periodic

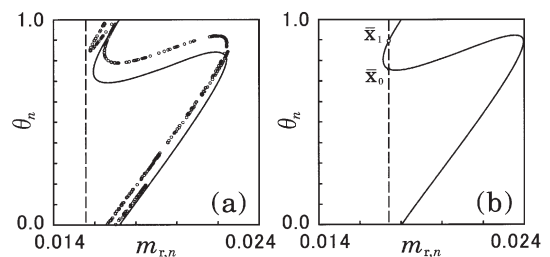


Fig. 5. I is shown as a dashed line and their images $\mathbf{M}(I)$ are shown as solid curves for forcing amplitude $A = 0.7$ and $\tau = 2$. (a) $v_0 = 0.78$; examples of chaotic orbits (open circles). (b) $v_0 = 0.80$; \bar{x}_0 is a stable fixed point.

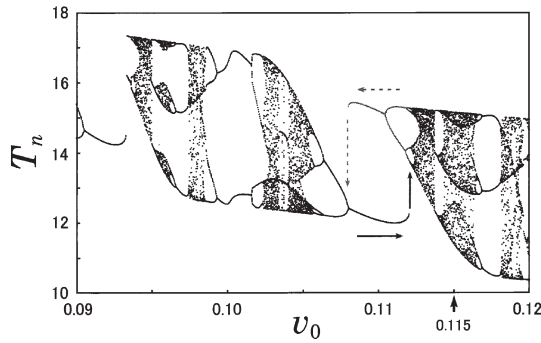


Fig. 6. Bifurcation diagram obtained from the mass-spring model without periodic forcing. $a = 0.916$. A hysteresis is observed depending on whether the flow velocity v_0 is increased or decreased, as indicated by arrows.

perturbations exhibit period doubling cascade to chaos.^{9-24,27} In addition, it was found both experimentally²¹ and theoretically⁹ that a unit structure which includes chaotic transitions repeatedly appears in bifurcation diagrams in a wide range of the flow rate for relatively large faucet radii. Figure 6 shows a typical unit structure in the bifurcation diagram calculated from the mass-spring model for the faucet radius $a = 0.916$ (2.5 mm), where no periodic perturbation is applied. Besides period doubling route to chaos, one can see, in Fig. 6, a hysteresis depending on whether v_0 is increased or decreased. Note that the hysteresis occurs in the transition point between two periodic orbits (instead of a periodic and a chaotic ones). In contrast, it turns out that the dripping faucet under periodic forcing exhibits another type of hysteresis which occurs in the transition point between periodic and chaotic motion when the forcing amplitude is varied for a fixed value of v_0 . In this section, the same parameter values as in ref. 9 have been employed: $a = 0.916$, $\gamma = 0.05$, $z_{crit} = 5.5$, $z_0 = 2.0$, $B = 0.2$, and $C = 0.3$, and the spring constant is assumed as

$$k(m) = \begin{cases} -11.4m + 52.5 & (m < 4.61) \\ 0 & (m \geq 4.61) \end{cases} \quad (3.1)$$

Now we apply a periodic force to the system in a chaotic state at $v_0 = 0.115$ [eq. (2.1)]. Figure 7(a) and 7(b) are bifurcation diagrams, where the forcing amplitude A is decreased in (a) and increased in (b). A sudden change

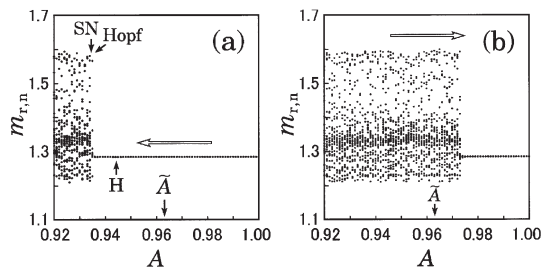


Fig. 7. Bifurcation diagram obtained from the mass-spring model with periodic forcing ($a = 0.916$, $v_0 = 0.115$, $\tau = 6$). Plot of the remnant mass at the breakup moment vs. forcing amplitude A . The final state at the present value of A is chosen as the initial state at the next value of A ; (a) A is decreased; (b) A is increased. The first 1000 points are discarded at each value of A . However, scattered points for $A > \bar{A}$ are transient because of very long transient times.

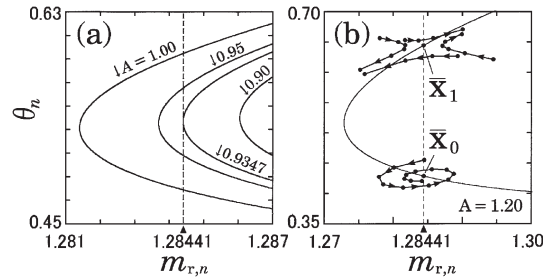


Fig. 8. (a) I is shown as a dashed line and their images $M(I)$ are shown as solid curves at various forcing amplitudes A . (b) Orbits near period-one orbits on the Poincaré section.

between chaotic and periodic motion occurs at a different value of A depending on whether the forcing amplitude is increased or decreased (hysteresis). To understand the discontinuous change of the oscillating state and the hysteresis, we analyze the Poincaré section in the two-dimensional space (m_r, θ) in detail. As discussed in §2, Fig. 8(a) illustrates how P1 orbits with $N = 2$ are generated as A is increased.

As A increases through $A = 0.9347$, I intersects $M(I)$. It was found numerically that two P1 orbits \bar{x}_0 and \bar{x}_1 , i.e., the intersection of I and $M(I)$, are generated via a saddle node bifurcation, where \bar{x}_1 is a saddle. The other fixed point \bar{x}_0 is a source (instead of sink) just after the saddle node bifurcation point. Therefore, there is only one attractor which is chaotic at this stage. It was found from a detailed analysis that the bifurcation of the 2-dimensional map of the present system can well be explained by a discretized version of a 2-dimensional flow which yields a homoclinic bifurcation: a scenario of a homoclinic bifurcation similar to that presented in ref. 28 can be applied, as shown in Figs. 9(a)–9(f). Figure 10 illustrates invariant manifolds of the Poincaré map (solid curves with arrows) together with numerical examples of orbits near the manifolds (dots and thin lines). The saddle node bifurcation point is presented in Fig. 10(a). As the parameter A increases, the unstable fixed point \bar{x}_0 is stabilized by a Hopf bifurcation [Fig. 10(b)]. The basin boundary of \bar{x}_0 is then an unstable limit cycle generated by the Hopf bifurcation. Further increase of A induces a homoclinic bifurcation [Fig. 10(c)]. Up to this stage, the basin of \bar{x}_0 is a small closed region. After the homoclinic bifurcation, the basin of \bar{x}_0 , whose boundary is a

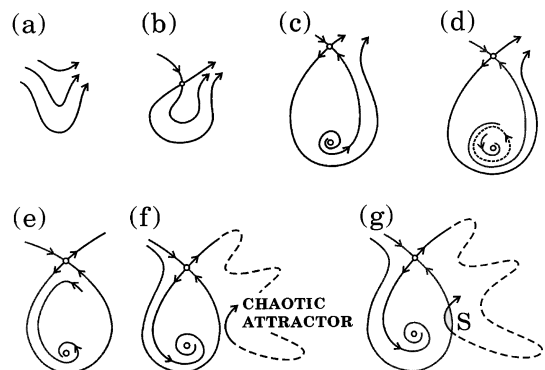


Fig. 9. Schematic of bifurcations.

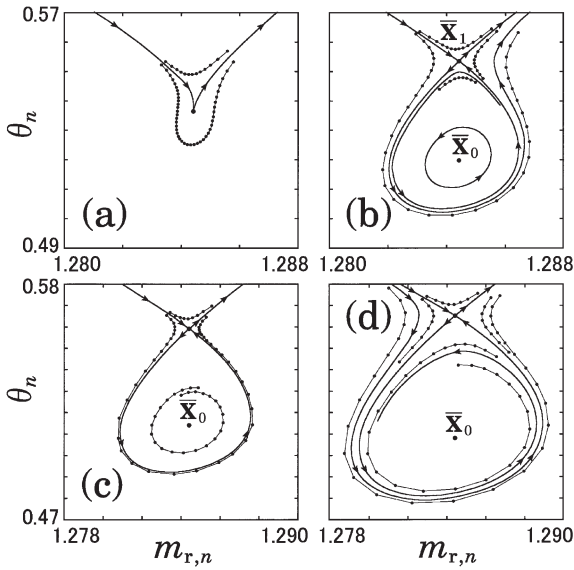


Fig. 10. Invariant manifolds (solid curves with arrows) and examples of orbits (dots and thin lines). $v_0 = 0.115$, $\tau = 6$. (a) $A = 0.9347$. (b) $A = 0.940$. (c) $A = 0.9441$. (d) $A = 0.950$.

heteroclinic orbit, is open. However, the chaotic attractor coexists and the motion remains chaotic, as shown in Fig. 11(a).

After A passes through a critical value $\tilde{A} = 0.963$, the chaotic attractor disappears via a boundary crisis due to a homoclinic tangency, and then the periodic motion \bar{x}_0 is realized. At the moment of the homoclinic tangency, the stable and unstable manifolds of \bar{x}_0 are tangent, which is the so called homoclinic tangency crisis.³¹⁾ The coexistence of the two attractors results in the hysteresis as shown in Fig. 11(a). If one starts from a large enough value of A [say $A = 1.2$ in 8(b)] at which the P1 motion is realized, and reduces the A value through \tilde{A} , the system keeps the P1 motion till the Hopf bifurcation occurs at $A \approx 0.936$. At a critical value $A = \tilde{A}$, the system exhibits the following scaling property:

$$n_t \sim (A - \tilde{A})^{-1.1} \quad \text{for } A > \tilde{A}, \quad (3.2)$$

where n_t is the average transient lifetime defined by the average iteration number before the orbit falls within a distance Δ ($= 10^{-3}$) from the stable P1 orbit [see Fig. 11(b)]. The average was taken over 25 initial points on the

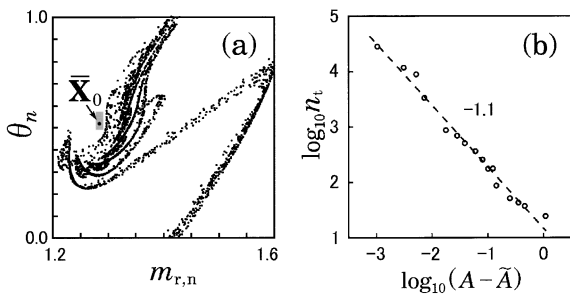


Fig. 11. (a) Poincaré section at $A = 0.950$. A stable fixed point \bar{x}_0 and the coexisting chaotic attractor. The gray rectangle corresponds to Fig. 10(d). (b) Log-log plot of the average transient lifetime n_t vs. $(A - \tilde{A})$, where $\tilde{A} = 0.963$.

Poincaré section. The exponent and the value of \tilde{A} were determined by least square fitting. As will be explained below, we conjecture that the critical exponent for two-dimensional maps can be estimated in terms of the information dimension D_1 of the original chaotic attractor just before the crisis as

$$\gamma \approx D_1 - \frac{1}{2}, \quad (3.3)$$

where $n_t \sim (A - \tilde{A})^{-\gamma}$. From eq. (3.3), one is suggested a relation between the critical exponent γ and the Lyapunov exponents of the chaotic set, because the Kaplan–Yorke conjecture connects D_1 to the Lyapunov exponents of the chaotic orbit.³³⁾ We numerically obtained $D_1 = 1.6$ for the chaotic set in Fig. 11(a) using the fixed mass approach.³⁰⁾ Thus γ is close to 1.1 as one can see in Fig. 11(b).

To derive the relation (3.3), let us consider the relative frequency that the chaotic transient orbit visits the small gray shaded region S in Fig. 9(g). Once the orbit gets into the region S , it rapidly converges to the stable fixed point \bar{x}_0 . As A increases and passes through the critical value \tilde{A} , the unstable manifold crosses the stable manifold as shown in Fig. 9(f) and 9(g), which is schematically illustrated as in Fig. 12. Let the width of the region S be p (note that $p \sim A - \tilde{A}$). By assuming the quadratic tangency, the area of S is estimated as $p \times \sqrt{p}$. Further, let us assume that the information dimension D_1 is regarded as the box-counting dimension of the smallest set that contains most of the attractor measure. (This has been proved, for example, in case of the generalized baker’s map^{32,33)}). When the chaotic attractor is covered with rectangles of the size $\sim p \times \sqrt{p}$, the number $N(p)$ of rectangles is given by

$$N(p) \sim p^{-(D_1-1)} \times (\sqrt{p})^{-1} = p^{-(D_1-\frac{1}{2})} \quad (3.4)$$

where we have assumed that the dimension of the attractor along the direction of the unstable manifold equals to unity. By assuming further an equal frequency that the orbit visits each rectangle, we obtain

$$n_t \sim N(p) \sim (A - \tilde{A})^{-(D_1-\frac{1}{2})}, \quad (3.5)$$

which yields (3.3). In Fig. 7(b), it should be noted that the chaotic orbit does not exist in the range $A > \tilde{A} = 0.963$. The scattered points of $m_{r,n}$ after A passed \tilde{A} is just transient.

The critical exponent of the chaotic transients was studied by Grebogi *et al.*³¹⁾ Although our approach is different from theirs, the values of γ which they obtained by numerical experiments on Ikeda map and Hénon map are in good agreement with γ obtained from eq. (3.3).

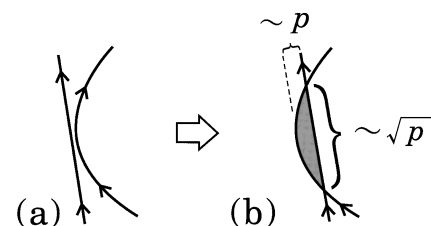


Fig. 12. Schematic diagram.

4. Fluid Dynamical Simulation

We have shown, using the mass-spring model, that the dripping faucet under periodic forcing undergoes a sudden discontinuous change between chaotic and periodic motion as the forcing amplitude is varied, and the transition point exhibits a hysteresis.

As mentioned already, the parameters of the mass-spring model have been determined from the corresponding fluid dynamical computations (FDC).^{9,22)} Naturally a transition similar to that observed in the mass-spring model should be expected for FDC, which we show in this section.

In the present FDC, we have perturbed the flow velocity as

$$v = v_0 \left(1 + \alpha \sin \left(\frac{2\pi t}{\tau} \right) \right), \quad (4.1)$$

in place of adding the periodic force. In case of FDC, the drop is not a point mass. Thus, the periodic perturbation applied to the top of the drop is better described in terms of the oscillation of the flow velocity (= the velocity of the top of the fluid) rather than the oscillating force which acts on the center of mass of the fluid.

Figure 13 is a bifurcation diagram for no periodic perturbation ($\alpha = 0$). The faucet radius is $a = 0.916$ (2.5 mm) and the viscosity is for the water at 20°C: $\eta = 0.002$ in units of $\eta_0 \equiv (\rho\Gamma^3/g)^{1/4}$. The unit structures of Fig. 13 and 6 exhibit several common characteristics: a period doubling, a period doubling cascade to chaos, a P2 motion in the middle of the unit, a transition between different periodic motions, the transition point which shows a hysteresis.

When the periodic perturbation is applied to a chaotic state at $v_0 = 0.095$ (see Fig. 13), the bifurcation diagram are obtained as Fig. 14(a) and 14(b). One can see sudden discontinuous changes between chaotic and periodic motion. A transition point exhibits a hysteresis, i.e., the change occurs at $\alpha = 0.043$ for increasing α , and at $\alpha = 0.38$ for decreasing α .

5. Conclusion

We have demonstrated from both the mass-spring model

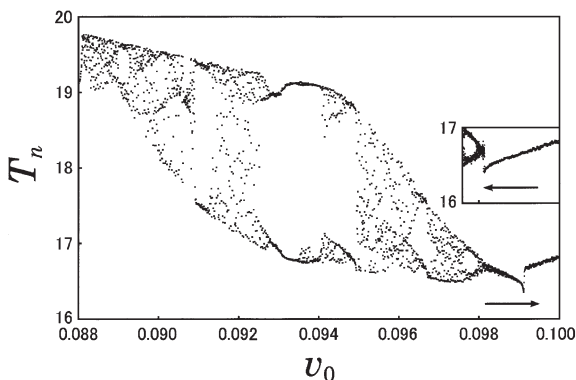


Fig. 13. Bifurcation diagram obtained from fluid dynamical computations. Plot of dripping time intervals T_n vs. flow velocity v_0 . A hysteresis is observed depending on whether the flow velocity v_0 is increased or decreased (inset).

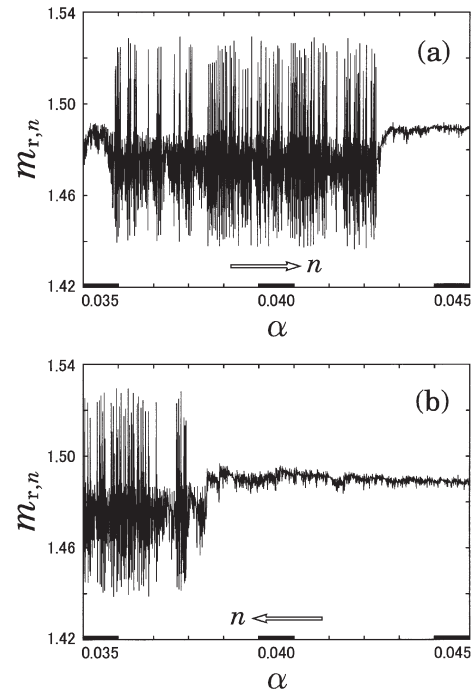


Fig. 14. Time series of the remnant mass at the breakup moment in a periodically forced system ($\tau = 8.7$). Forcing amplitude α is (a) increased and (b) decreased, where α is varied for every 100 drops.

and the fluid dynamical computation that periodic forcing induces transitions between chaotic and periodic motion in the dripping faucet system. Since the dimension of the dynamical system generally increases by 1.0 by an external perturbation, a saddle node bifurcation can occur, which is not inherent in the original dynamics of the dripping faucet. Global bifurcations following the saddle node bifurcation are the origin of the discontinuous change from a chaotic to a periodic state.

Postnov *et al.*³⁴⁾ analyzed a periodically forced 4-dimensional flow, and found that a torus coexists with a stable periodic orbit between a saddle node bifurcation and a homoclinic one. In the present system, in contrast, chaos coexists with a stable periodic orbit between a Hopf bifurcation and a homoclinic one.

It is interesting to note that a similar structure of the Poincaré section as in Fig. 10(d) was observed in a dripping faucet experiment by Pinto and Sartorelli,²³⁾ although no periodic force was applied. The present analysis suggests that their result may possibly be explained if any oscillatory factor was generated inevitably in the experimental condition.

Taming chaos in the dripping faucet is to stabilize the system to obtain drops of the same size, which might be practically important. We have suggested the possibility to stabilize the system in terms of external periodic forcing.

We thank Professor M. Shoji for permission to copy his figure. This research was partly supported by Iketani Science and Technology Foundation.

- 1) T. Kapitaniak: *Controlling Chaos* (Academic Press, San Diego, 1996) and references therein.
- 2) E. Ott, C. Grebogi and J. A. Yorke: *Phys. Rev. Lett.* **64** (1990) 1196.

- 3) Y. Braiman and I. Goldhirsch: Phys. Rev. Lett. **66** (1991) 2545.
- 4) T. Tamura, N. Inaba and J. Miyamichi: Phys. Rev. Lett. **83** (1999) 3824.
- 5) K. A. Mirus and J. C. Sprott: perturbations, Phys. Rev. E **59** (1999) 5313.
- 6) Z. Qu, G. Hu, G. Yang and G. Qin: Phys. Rev. Lett. **74** (1995) 1736.
- 7) H.-T. Su, Y.-H. Chen and R.-R. Hsu: Phys. Rev. E **59** (1999) 4687; R.-R. Hsu, H.-T. Su, J.-L. Chern and C.-C. Chen: Phys. Rev. Lett. **78** (1997) 2936.
- 8) H.-J. Li and J.-L. Chern: Phys. Rev. E **54** (1996) 2118.
- 9) K. Kiyono and N. Fuchikami: J. Phys. Soc. Jpn. **68** (1999) 3259.
- 10) R. Shaw: *The Dripping Faucet as a Model Chaotic System* (Aerial Press, Santa Cruz, 1984); P. Martien, S. C. Pope, P. L. Scott and R. S. Shaw: Phys. Lett. A **110** (1985) 399.
- 11) H. N. N. Yépez, A. L. S. Brito, C. A. Vargas and L. A. Vicente: Eur. J. Phys. **10** (1989) 99.
- 12) X. Wu and Z. A. Schelly: Physica D **40** (1989) 433.
- 13) K. Dreyer and F. R. Hickey: Am. J. Phys. **59** (1991) 619.
- 14) J. Austin: Phys. Lett. A **155** (1991) 148.
- 15) J. C. Sartorelli, W. M. Gonçalves and R. D. Pinto: Phys. Rev. E **49** (1994) 3963.
- 16) R. D. Pinto, W. M. Gonçalves, J. C. Sartorelli and M. J. de Oliveira: Phys. Rev. E **52** (1995) 6896.
- 17) T. J. P. Penna, P. M. C. de Oliveira, J. C. Sartorelli, W. M. Gonçalves and R. D. Pinto: Phys. Rev. E **52** (1995) R2168.
- 18) M. S. F. da Rocha, J. C. Sartorelli, W. M. Gonçalves and R. D. Pinto: Phys. Rev. E **54** (1996) 2378.
- 19) J. G. M. da Silva, J. C. Sartorelli, W. M. Gonçalves and R. D. Pinto: Phys. Lett. A **226** (1997) 269.
- 20) R. D. Pinto, W. M. Gonçalves, J. C. Sartorelli, I. L. Caldas and M. S. Baptista: Phys. Rev. E **58** (1998) 4009.
- 21) T. Katsuyama and K. Nagata: J. Phys. Soc. Jpn. **68** (1999) 396.
- 22) N. Fuchikami, S. Ishioka and K. Kiyono: J. Phys. Soc. Jpn. **68** (1999) 1185.
- 23) R. D. Pinto and J. C. Sartorelli: Phys. Rev. E **61** (2000) 342.
- 24) G. I. Sánchez-Ortiz and A. L. Salas-Brito: Phys. Lett. A **203** (1995) 300; G. I. Sánchez-Ortiz and A. L. Salas-Brito: Physica D **89** (1995) 151.
- 25) A. D'Innocenzo and L. Renna: Phys. Rev. E **58** (1998) 6847; Phys. Lett. A **220** (1996) 75; *ibid.* **220** (1996) 75.
- 26) L. Renna: Phys. Lett. A **261** (1999) 162.
- 27) M. Shoji: Nonlinear characteristics in dripping faucet, 5th Int. Workshop on Chaos/Turbulence/Complex Systems, Tsukuba, November 6, 1998.
- 28) S. Wiggins: *Introduction to Applied Nonlinear Dynamical Systems and Chaos* (Springer-Verlag, New York, 1990).
- 29) A. Ilarraza-Lomel, C. M. Arizmendi, A. L. Salas-Brito: Phys. Lett. A **259** (1999) 115.
- 30) R. Hegger, H. Kantz and T. Schreiber: Chaos **9** (1999) 413.
- 31) C. Grebogi, E. Ott and J. A. Yorke: Phys. Rev. Lett. **57** (1986) 1284.
- 32) J. D. Farmer, E. Ott and J. A. Yorke: Physica D **7** (1983) 153.
- 33) E. Ott: *Chaos in dynamical systems* (Cambridge University Press, New York, 1993) 134.
- 34) D. E. Postnov, A. G. Balanov, N. B. Janson and E. Mosekilde: Phys. Rev. Lett. **83** (1999) 1942.